Atomic-Level Processes of Shear Band Nucleation in Metallic Glasses

D. Şopu,[1,*] A. Stukowski,[2] M. Stoica,[3] and S. Scudino[1]
[1]Institute for Complex Materials, IFW Dresden, Helmholtzstraße 20, D-01069 Dresden, Germany
[2]Institut für Materialwissenschaft, Technische Universität Darmstadt, Otto-Berndt-Strasse 3, D-64287 Darmstadt, Germany
[3]Laboratory of Metal Physics and Technology, Department of Materials, ETH Zurich, 8093 Zurich, Switzerland
(Received 17 July 2017; published 9 November 2017)

The ability to control the plastic deformation of amorphous metals is based on the capacity to influence the percolation of the shear transformation zones (STZs). Despite the recent research progress, the mechanism of STZ self-assembly has so far remained elusive. Here, we identify the structural perturbation generated by an STZ in the surrounding material and show how such a perturbation triggers the activation of the neighboring STZ. The mechanism is based on the autocatalytic generation of successive strong strain and rotation fields, leading to STZ percolation and, ultimately, to the formation of a shear band.

DOI: 10.1103/PhysRevLett.119.195503

In contrast to conventional polycrystalline materials, which deform plastically through dislocation activity, plastic deformation in metallic glasses occurs by the activation of shear transformation zones (STZs): clusters of close-packed atoms that cooperatively reorganize under the action of an applied stress to form highly localized shear bands [1,2]. Because of the fast dynamics and localized nature of shear banding [3,4], the atomistic mechanism of plastic deformation in amorphous metals cannot be properly resolved by experimental means yet, and investigations of this crucial aspect have relied so far on computer simulations, a powerful tool to study the atomic-level mechanism of shear band formation.

Simulations reveal that STZs are preferentially activated in regions involving weakly bonded atoms, where the most geometrically unfavored motifs would experience the largest nonaffine strains [5–7]. Earlier simulations indicate that STZs induce quadrupolar elastic displacements in the surrounding matrix, behaving as Eshelby inclusions [8], and, recently, it has been suggested that the alignment of Eshelby-like quadrupoles may cause the density variation observed in shear bands [9]. The interaction between these long-range elastic fields can induce transient strain localization events reminiscent of shear bands [10]; STZs are thus not independent, random events but may occur as directional quasilinear avalanches [11]. As a result of the long-range interactions, it is generally postulated that STZs may start percolating along a viable plane of maximum shear stress, eventually leading to the formation of shear bands [2]; the mechanism leading to STZ percolation is, however, not fully established yet, and key aspects, such as the structural characteristics of the perturbation generated by an STZ in the surrounding material and how such a perturbation triggers the activation of the neighboring STZ, have still to be clarified. Here, by analyzing the most striking structural features characterizing the STZs and the material between adjacent STZs in a simulated $Cu_{64}Zr_{36}$ metallic glass, we identify the atomic-level mechanism underlying the STZ percolation process. Our findings have major implications for understanding the dynamics of STZ activation and, consequently, for controlling shear band formation and propagation in metallic glasses and other disordered materials.

The mechanism of shear banding in the $Cu_{64}Zr_{36}$ metallic glass was analyzed by molecular dynamics (MD) simulations using the code LAMMPS [12] and the Finnis-Sinclair–type potential developed by Mendelev, Sordelet, and Kramer [13]. The simulated specimen was generated as follows. First, a metallic glass cubic cell containing 8000 atoms was produced by quenching it from the melt to 50 K with a cooling rate of 10^{10} K/s. A rectangular sample with dimensions $46 \times 5 \times 106$ nm^3 was then created by replicating the initial glass cubic cell, giving a total number of atoms of about 1.5×10^6 (see Supplemental Material [14], Fig. S1).

In order to ensure that the plastic deformation is confined to a single shear band and to control its position and propagation path, a stress concentrator was created at the surface of the specimen by extruding a small notch in the plane. The notched sample was loaded under uniaxial tension along Z using a constant strain rate of 4×10^7 1/s. To guarantee a regime of localized deformation despite the high strain rate used, the simulations were carried out at a low, constant temperature of 50 K [15]. This approach is specific for the behavior observed in simulations, which employs ultrafast strain rates. Periodic boundary conditions were applied along the Y and Z directions, while the free surface condition was used along the X axis. The atomic von Mises strain, volumetric strain, local deviation from affine deformation (D^2_{min}) [16], rotation angle, the atomic Green-Lagrangian strain tensor, and also Voronoi polyhedra were calculated and visualized using the OVITO software [17]. The aforementioned micromechanical quantities are evaluated at each atomic site from the relative motion of the neighboring atoms within a cutoff range of 10 Å. First, the atomic

 © 2017 American Physical Society

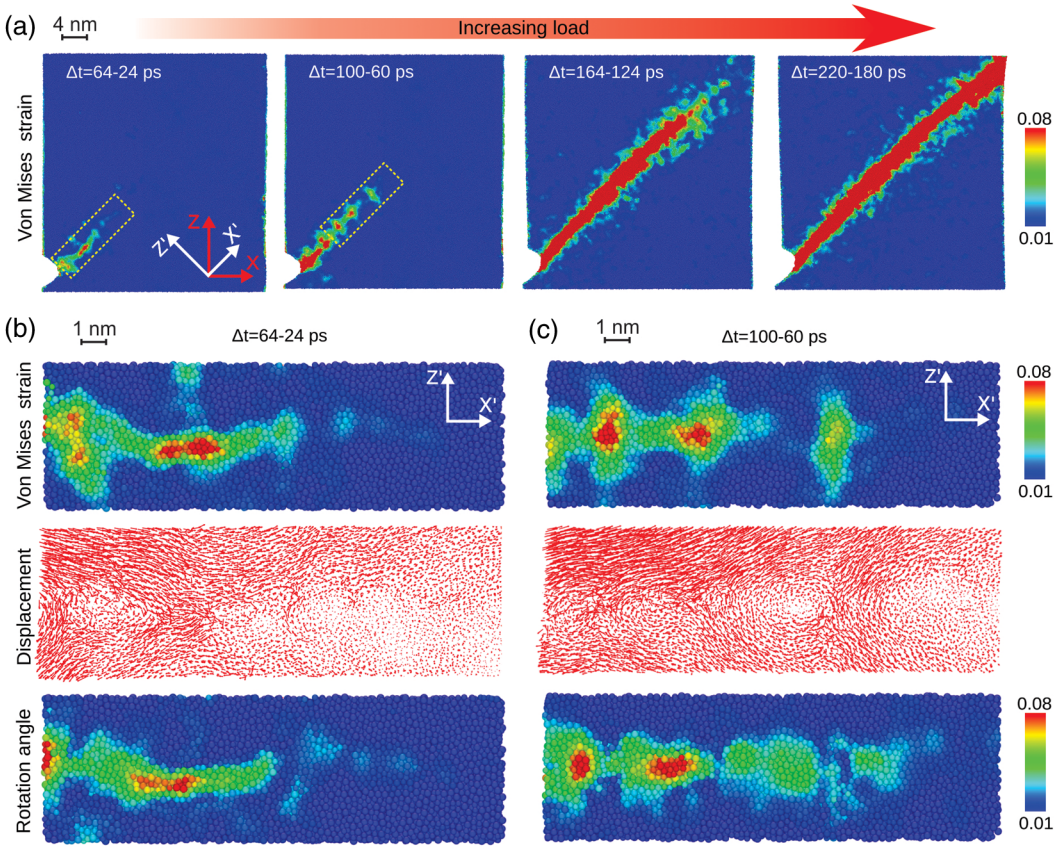

FIG. 1. Structural variations in the simulated $Cu_{64}Zr_{36}$ metallic glass during the early stages of shear banding. (a) Overall evolution of the atomic von Mises strain built up within consecutive time frames of 40 ps. von Mises strain, displacement, and rotation angle (radians) in the areas corresponding to the dotted boxes in (a) for the time frames (b) $\Delta t_1 = 64 - 24$ ps and (c) $\Delta t_2 = 100 - 60$ ps.

deformation gradient F is computed using a least-squares fit to the atomic displacement vectors [18]. Next, derived metrics are calculated from F, such as the Green-Lagrangian strain tensor and its volumetric and von Mises invariants. The polar decomposition $F = RU$ yields the microrotation matrix R [19] and the corresponding angle of rotation. The per-atom stress tensor for each atom in the system was computed by LAMMPS [12]. The von Mises strain, volumetric strain, $D^2_{\min}$, rotation angle, and von Mises stress along the X' axis and the eigenvectors plotted along the Z' axis are average values calculated within consecutive small volumes with size of about $1.5 \times 1 \times 1.5$ nm^3 containing ~50 atoms.

Figure 1(a) shows the evolution of the atomic von Mises strain building up within short time frames of 40 ps evaluated by MD simulations. The strain evolution shows the characteristic features of shear banding in simulated metallic glasses: The shear band is initiated at the notch root, where the stress is concentrated, and propagates along a plane of maximum resolved shear stress. The strain distribution within the evolving shear band is initially highly discontinuous, consisting of isolated regions of larger strain. To understand the origin of such a discontinuous behavior, we have focused our investigation on the tip of the developing shear band during the first two time frames $\Delta t_1 = 64 - 24$ ps and $\Delta t_2 = 100 - 60$ ps [Figs. 1(b) and 1(c)]. The atomic displacement vectors reveal the presence of regions where atoms describe circular displacements resembling a collective, vortexlike motion. Such a vortexlike flow corresponds to a strong rigid rotation of the groups of atoms and appears as a signal in the computed microrotation field [Figs. 1(b) and 1(c), bottom panels]. A representative vortex is considered in Figs. 2(a) and 2(b): The magnitude of the displacements increases from the core to the outer shell of the vortex, whereas the rotation angle exhibits an opposite trend.

Vortex formation is a common feature of shear banding in other disordered materials, such as granular matter [20]. The question that naturally arises here is whether the observed vortexes and the associated rotation are integral parts of the STZs. Moreover, could vortex flow control the activation and percolation of STZs and thus the formation of shear bands in metallic glasses? To answer these questions, the structure of the vortexes has been analyzed in detail, as will be discussed below.

The common topological feature in Cu-rich Cu-Zr metallic glasses is the dominance of the Cu-centered full-icosahedral (FI) cluster [21]. The fraction of FI clusters is

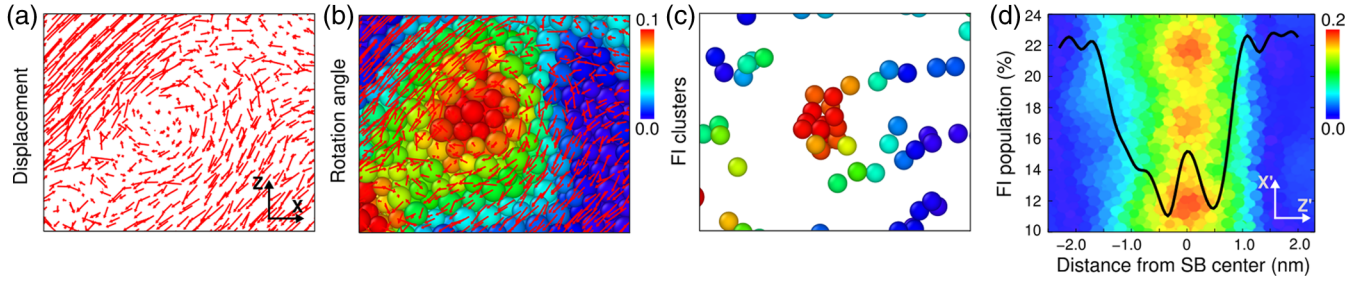

FIG. 2. (a) Representative vortex described by the displacement vectors and (b) displacement vectors and corresponding angle of rotation (color code). (c) The vortex is centered on a high population of FI clusters and are surrounded by distorted clusters (not shown here; only FI clusters colored according to their angle of rotation are displayed in the figure). (d) Average population of FI clusters across the shear band and characteristic contour map showing the angle of rotation (radians).

drastically reduced within the shear bands, where highly distorted and fragmented clusters form [22]. The destruction of FI clusters and the corresponding increase of more compliant disordered clusters make the shear band less able to resist shear, which in turn leads to autocatalytic shear softening and strain accumulation within the band [22]. Here, we observe a large number of FI clusters in the center of the vortexes [Fig. 2(c)]. As already reported by Cao, Cheng, and Ma [22], the fraction of FI units decreases across the shear band from about 22% in the outer elastic matrix to 11% within the shear band [black curve in Fig. 2(d)]; however, when approaching the shear band core, the FI population increases again to about 15%. In other words, the destruction of the FI backbone necessary for flow localization [22] does not occur uniformly within the shear band, and small islands of FI clusters survive. These stiff and tightly packed icosahedral clusters form the vortex centers of rotation. Distorted icosahedral clusters [missing atoms in Fig. 2(c)] surround the vortex cores and connect them to the undeformed matrix.

Strong rotation and strain fields appear to be mutually exclusive [Figs. 1(b) and 1(c)]: Areas with the largest rotation display reduced von Mises strain, whereas strong strain coincides with smaller rotation. The mechanism of shear band formation thus entails two main units: entities characterized by strong strain and vortexlike (rotating) structures. A new question arises here: Do heavily strained areas and vortexes constitute an STZ? The conventional definition of STZs as clusters of atoms that rearrange in response to the applied stress is rather broad and does not permit one to recognize such units of plasticity accurately. This is a fundamental aspect to clarify in order to understand STZ percolation.

In order to overcome this limitation, in their seminal work, Falk and Langer [16] used the local deviation from affine deformation (D^2_{min}) as a diagnostic for identifying an irreversible shear transformation at the atomic level. The same tool is used here. Plotting the value of D^2_{min} in the forming shear band as a function of the distance from the shear band tip [Fig. 3(a)] reveals several peaks of nonaffine deformation, which are offset by a background that monotonically decreases toward the tip [dashed blue line in Fig. 3(a)]. These peaks coincide with the maxima of the von Mises strain in Fig. 3(b) and represent the positions of distinct STZs. The STZs identified in this manner correspond to maxima of volumetric strain [Fig. 3(c)], in agreement with the dilatation required for STZ activation [4]. The STZs are separated by vortexes [Fig. 3(e)]—regions with a large rotation angle and relatively lower volumetric strain that becomes even negative at the shear band tip. This atomic motion generates an alternating sequence of STZ and vortex

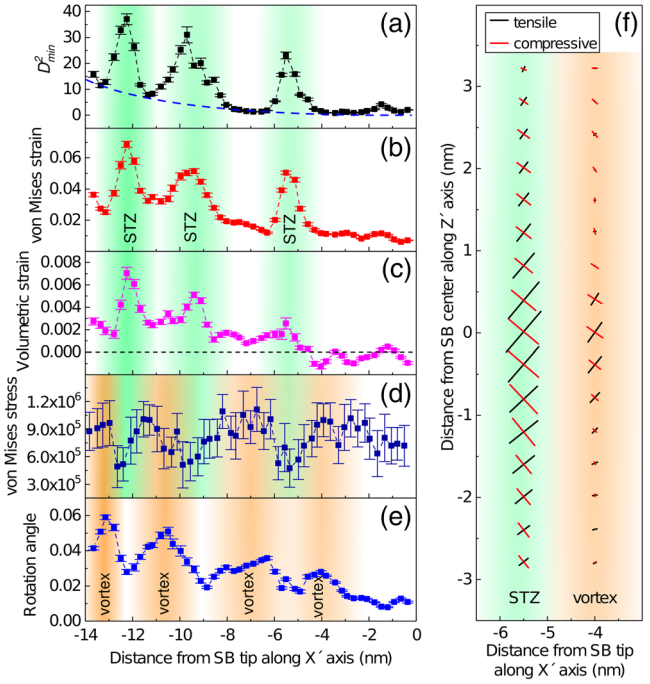

FIG. 3. Values along the shear band (SB) direction of the deviation from affine deformation, D^2_{min} (a), von Mises strain (b), volumetric strain (c), von Mises stress (unit, atm × Å^3) (d), and rotation angle (e) for $\Delta t_2 = 100 - 60$ ps, averaged across the band. The dashed blue line in (a) marks the decreasing background used to identify the STZs. (f) Variation of the eigenvectors of the strain tensor across the shear band for the STZ-vortex combination at the shear band tip. The position of the shear band tip is defined where the monotonically decreasing background [dashed blue line in (a)] reaches $D^2_{\mathrm{min}} = 0$.

elements along the shear band, characterized by a rather systematic variation of the stress: The stress is minimum at the STZs, whereas the vortexes display relatively higher stresses [Fig. 3(d)]. The sequence is initiated at the notch by an STZ (see Supplemental Material [14], Fig. S2), is immediately followed by a region with strong rotation, and ends with a vortex at the shear band tip [Fig. 3(e)]. The structural perturbation resulting from the activation of an STZ thus causes the rotation observed in the neighboring undeformed matrix, which in turn appears to be a necessary step to activate the following STZ through a type of autocatalytic process.

Having identified the recurring units within a developing shear band and their chronological and spatial sequence, it is now possible to discuss the mechanism leading to STZ percolation with the help of the schematic representation in Fig. 4, which shows the consecutive activation of two neighboring STZs near a notch. Here, we assume the glassy structure to consist of a FI backbone, which needs to be

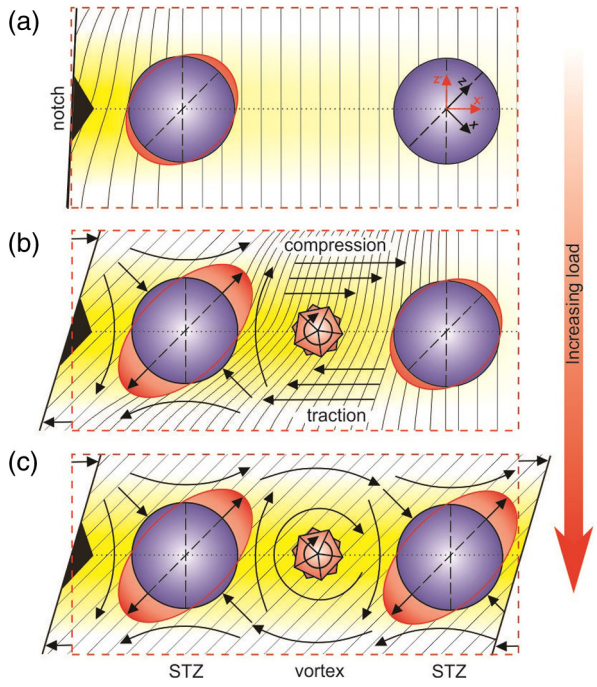

FIG. 4. Schematic representation of the STZ percolation mechanism. At small loads (a), the STZ near the notch experiences some degree of distortion with a negligible effect on the neighboring matrix. The STZ is activated at a higher load (b), generating a strong antisymmetric stress field in the FI-rich adjacent material, which in turn causes a collective vortexlike motion. This motion already induces some first deformation in the neighboring STZ, and, once the stress exceeds the threshold value, the following STZ is activated (c). The repetition of this two-unit STZ-vortex mechanism leads to STZ percolation along a specific direction and, ultimately, to the formation and propagation of a shear band. The nonactivated STZs are represented by purple circles, whereas STZ distortions are depicted by orange ellipses. The black arrows indicate atomic motion.

locally altered to induce strain localization, as proposed by Cao, Cheng, and Ma [22]. Although STZs cannot be identified *a priori* as topological defects [4], it is plausible that areas with a larger free volume and/or liquidlike clusters may initially experience some degree of distortion with a negligible effect on the surrounding matrix [Fig. 4(a)]. At higher loads [Fig. 4(b)], the stress at these favorable sites may exceed the threshold value required for STZ activation [2]: The FI backbone is locally broken (Fig. 2), and the STZ distortion results in a net volumetric increase [Fig. 3(c)]. The area ahead of the activated STZ is, in contrast, characterized by strong rotation and comparatively lower von Mises and volumetric strains. Such a vortexlike structure exhibits a relatively high fraction of stiff FI clusters in its center (Fig. 2) and, in the mechanism proposed here, represents the medium transmitting the structural distortion to the following STZ.

The effect of the vortexes can be understood by inspecting Fig. 3(f), which displays the variation of the eigenvectors of the strain tensor across the shear band for the STZ-vortex combination at the shear band tip. The orientation of the STZ distortion is not random: The tensile strain is oriented along the loading direction, whereas the compressive strain is perpendicular to it. The STZ activation perturbs the area around the adjacent vortex by generating a strong antisymmetric strain field. The tensile strain compresses the material above the vortex, and the compressive field generates traction below it [Figs. 3(f) and 4(b)]. In analogy to Eshelby's description of an inclusion, such a compression-traction strain field may be viewed as the long-range effect of the quadrupolar elastic field induced by the STZ in the surrounding material. The propensity for atomic rearrangement within an STZ is most likely directional [3]: STZs favorably oriented with the applied load will be more easily activated than STZs with unfavorable orientations, locally inducing the destruction of the FI arrangement. This hypothesis is corroborated by the STZ distortion oriented with the applied load observed in Fig. 3(f). On the other hand, the principal strain axes at the two sides of the vortex are unfavorably oriented. This misorientation might act as confinement, reducing the tendency for damaging of the FI backbone that, in contrast, occurs in a favorably oriented STZ. This interpretation would explain why highly packed icosahedral clusters are retained in the vortex cores. The transmission of the STZ distortion to the following STZ is thus mediated by the antisymmetric strain field in conjunction with the rotation of the FI stiff clusters, as in a ball-bearing-like arrangement, and is most likely stress driven. In contrast to the STZs, where the stress is locally relaxed [Fig. 3(d)], the region between the STZs displays comparatively higher stresses and is thus able to store the energy necessary to activate the next STZ. The stress progressively accumulated in this region initially induces some deformation in the adjacent STZ [Fig. 4(b)], and,

once it exceeds the threshold value, the STZ is activated and distorted along the favorable orientation [Fig. 4(c)]. The reiteration of these unit steps leads to STZ percolation along a specific direction and, ultimately, to the formation of a shear band.

In conclusion, we have identified a two-unit mechanism providing an atomistic description of the catalytic self-assembly of STZs. We suggest that our results may have significant implications for understanding several aspects characterizing the process of shear banding in metallic glasses and other disordered materials. For example, the negative volumetric strain (i.e., shrinking) at the shear band tip is in agreement with the density variations experimentally observed within a shear band [9,23], whereas the variation of the strain direction identified here at the nanoscale has been observed by x-ray diffraction to span over several micrometers [24]. Additionally, we expect our analysis to bring together the two scenarios of homogeneous versus heterogeneous shear band nucleation from structural fluctuations or extrinsic flaws [3]. Finally, through the proper control of the STZ-vortex sequence, one could handle the shear band dynamics and avoid runaway instability, thereby improving the plastic deformability of metallic glasses at room temperature, the key to the extensive use of these attractive materials in structural and functional applications.

D.S. acknowledges the financial support by the Deutsche Forschungsgemeinschaft (DFG) through Grant No. SO 1518/1-1. The authors gratefully acknowledge the computing time granted by the John von Neumann Institute for Computing (NIC) and provided on the supercomputer JURECA at the Juelich Supercomputing Centre (JSC). Additional computing time was made available by the Center for Information Services and High Performance Computing (ZIH) at TU Dresden. The authors thank U. Nitzsche for technical assistance concerning the computer simulations.

*Present address: Institut für Materialwissenschaft, Technische Universität Darmstadt, Otto-Berndt-Strasse 3, D-64287 Darmstadt, Germany; Erich Schmid Institute of Materials Science, Austrian Academy of Sciences, Jahnstraße 12, A-8700 Leoben, Austria.
Corresponding author.
sopu@mm.tu-darmstadt.de

[1] A. S. Argon, Acta Metall. **27**, 47 (1979).
[2] C. A. Schuh and A. C. Lund, Nat. Mater. **2**, 449 (2003).
[3] A. L. Greer, Y. Q. Cheng, and E. Ma, Mater. Sci. Eng. R **74**, 71 (2013).
[4] C. A. Schuh, T. C. Hufnagel, and U. Ramamurty, Acta Mater. **55**, 4067 (2007).
[5] J. Ding, S. Patinet, M. L. Falk, Y. Cheng, and E. Ma, Proc. Natl. Acad. Sci. U.S.A. **111**, 14052 (2014).
[6] E. Ma, Nat. Mater. **14**, 547 (2015).
[7] H. W. Sheng, W. K. Luo, F. M. Alamgir, J. M. Bai, and E. Ma, Nature (London) **439**, 419 (2006).
[8] V. V. Bulatov and A. S. Argon, Model. Simul. Mater. Sci. Eng. **2**, 167 (1994).
[9] V. Hieronymus-Schmidt, H. Rösner, G. Wilde, and A. Zaccone, Phys. Rev. B **95**, 134111 (2017).
[10] C. Maloney and A. Lemaître, Phys. Rev. Lett. **93**, 016001 (2004).
[11] A. Lemaître and C. Caroli, Phys. Rev. Lett. **103**, 065501 (2009).
[12] S. J. Plimpton, Comput. Phys. **117**, 1 (1995).
[13] M. I. Mendelev, D. J. Sordelet, and M. J. Kramer, J. Appl. Phys. **102**, 043501 (2007).
[14] See Supplemental Material at http://link.aps.org/supplemental/10.1103/PhysRevLett.119.195503 for sample shape and coordinate system, and for shear band nucleation at the notch.
[15] K. Albe, Y. Ritter, and D. Şopu, Mech. Mater. **67**, 94 (2013).
[16] M. L. Falk and J. S. Langer, Phys. Rev. E **57**, 7192 (1998).
[17] A. Stukowski, Modelling Simul. Mater. Sci. Eng. **18**, 015012 (2010).
[18] F. Shimizu, S. Ogata, and J. Li, Mater. Trans., JIM **48**, 2923 (2007).
[19] G. J. Tucker, J. A. Zimmerman, and D. L. McDowell, Int. J. Eng. Sci. **49**, 1424 (2011).
[20] J. M. Padbidri, C. M. Hansen, S. Dj. Mesarovic, and B. Muhunthan, J. Appl. Mech. **79**, 031011 (2012).
[21] Y. Q. Cheng, E. Ma, and H. W. Sheng, Phys. Rev. Lett. **102**, 245501 (2009).
[22] A. J. Cao, Y. Q. Cheng, and E. Ma, Acta Mater. **57**, 5146 (2009).
[23] V. Schmidt, H. Rösner, M. Peterlechner, G. Wilde, and P. M. Voyles, Phys. Rev. Lett. **115**, 035501 (2015).
[24] H. S. Shahabi, S. Scudino, I. Kaban, M. Stoica, B. Escher, S. Menzel, G. B. M. Vaughan, U. Kühn, and J. Eckert, Acta Mater. **111**, 187 (2016).